Construction and Building Materials 238 (2020) 117672

Contents lists available at ScienceDirect

Construction and Building Materials

journal homepage: www.elsevier.com/locate/conbuildmat

Autogenous healing of Engineered Cementitious Composites (ECC) based on MgO-fly ash binary system activated by carbonation curing

Duo Zhang [a], Haoliang Wu [b], Victor C. Li [a], Brian R. Ellis [a,*]

[a] Department of Civil and Environmental Engineering, University of Michigan, Ann Arbor, MI 48109, United States
[b] Jiangsu Key Laboratory of Urban Underground Engineering & Environmental Safety, Institute of Geotechnical Engineering, Southeast University, Nanjing, China

HIGHLIGHTS

- Rapid self-healing of carbonation-cured MgO-based PC-free ECC was demonstrated.
- Healing of microcracks occurred primarily at the crack surface.
- Tensile strength and ductility are not fully restored after self-healing.
- Nesquehonite was the primary mineral phase filling healed crack openings.

ARTICLE INFO

Article history:
Received 25 June 2019
Received in revised form 18 September 2019
Accepted 21 November 2019

Keywords:
Engineered Cementitious Composites (ECC)
Carbonation curing
CO_2 utilization
Self-healing
MgO cement

ABSTRACT

Developing self-healing of concrete cracks represents a critical approach for extending material longevity. If demonstrated on concretes with CO_2 stored through carbonation curing, self-healing can further mitigate infrastructure lifecycle emissions. In this study, the self-healing process is investigated on novel Engineered Cementitious Composites (ECC) based on binary blends of reactive MgO cement and siliceous fly ash activated by carbonation. The self-healing was observed under cyclic wetting and drying exposures and was characterized by measurements of resonance frequency, optical microscopy and X-ray computed microtomography (XCT). Thermogravimetric analysis, X-ray powder diffraction and scanning electron microscopy were employed to assist in identifying healing products and mechanisms. It was found that micro-cracks could be autogenously filled in 7 wet-dry cycles, as evidenced by over 95% recovery of resonance frequency and healed crack appearance under optical microscopic observation. Nevertheless, the composite mechanical performance, particularly tensile strength and ductility, did not fully recover with respect to the uncracked specimens. The inadequate post-healing mechanical properties were consistent with XCT observations that indicated low material densities in the cracked area. Based on the chemical and microstructural characterizations, it was determined that nesquehonite crystallites were responsible for the crack filling. Although the nesquehonite filled cracks will be less permeable to invasion of reactive fluids, novel strategies are needed to establish more robust healing capability to completely restore the crack bridging and composite tensile performance.

1. Introduction

Concrete is the world's single most used construction material, with a global production of more than 10 billion tons each year [1]. Manufacturing of Portland cement (PC), the bonding ingredient predominantly used for concrete, accounts for about 5% of global anthropogenic CO_2 emissions [2]. The increasing need for new construction across the globe highlights the urgency for developing novel materials and manufacturing approaches that are more sustainable and less carbon intensive. One emerging strategy is to reduce the use of PC by introducing reactive MgO cement as a potential alternative binder coupled with direct CO_2 sequestration through CO_2-curing [3,4]. MgO cement is a low energy cementitious material that has a widely distributed feedstock and high reactivity for CO_2 carbonation [5,6]. At calcining temperatures of 700–1000 °C, the hydraulic potential of MgO minerals can be preserved, and once in contact with water, MgO hydrates to form brucite ($Mg(OH)_2$). This hydration process does not generate sufficient binding properties or strength and is therefore not capable of carrying structural loads needed for construction applications. Carbonation curing, however, can be used to activate the binding

* Corresponding author.
E-mail address: brellis@umich.edu (B.R. Ellis).

https://doi.org/10.1016/j.conbuildmat.2019.117672
0950-0618/

property of MgO by converting brucite to a series of hydrated magnesium carbonates (HMCs), such as hydromagnesite, lansfordite and nesquehonite [7], with varying stoichiometry of bound water, carbonate and hydroxyl components [8–10]. The chemical formulations of the reactive MgO cement can be engineered with supplementary cementitious materials and chemical/mineral additives to promote the CO_2 carbonation process, which can lead to comparable or even superior concrete strengths with respect to conventional PC-based products [11]. This carbonation-formed strength is largely originated from the increase in solid volume and network binding structure through carbonate crystals [12]. In prior work, use of reactive MgO cement has mostly been applied to the production of precast concrete, which often combines PC [13–15], fly ash [16,17], and ground granulated blast furnace slag [18] to form blended binding phases.

Engineered Cementitious Composites (ECC) is a class of ultraductile and highly durable construction materials [19]. Unlike the brittle concrete or tension-softening fiber-reinforced cementitious composites, ECC shows strain-hardening behavior under tension and forms multiple fine cracks rather than a single wide crack to accommodate imposed large tensile strains. The tight crack width is an intrinsic material property of the ECC and can be autogenously maintained within specific ranges irrespective of loading or deformation. This is a unique feature of ECC, which maintains low material permeability even at cracked states. Tight crack width and ultrahigh ductility collectively make ECC highly durable and resilient under static and impact loading conditions, leading to reductions in life-cycle carbon emissions and cost [20]. The high binder content in ECC offers a substantial opportunity for utilization of reactive MgO cement combined with CO_2 curing and has motivated the development of a novel version of ECC built upon the MgO-fly ash-CO_2 system [21,22]. This novel MgO-ECC attains a tensile strain capacity of more than 5% and sequesters ~ 30% CO_2 by mass of MgO within 24 h, offering new infrastructure applications for the carbonated MgO cement.

Cracking is one of the main forms of deterioration in concrete structures [23]. Cracks can be generated at nearly every stage of material service life, potentially due to effects such as shrinkage, mechanical loading, and thermal gradients. Above 0.1 mm, cracks could drastically accelerate the ingress of harmful species that lead to premature material and structural deterioration [24]. As one of the emerging strategies countering such deterioration, self-healing of concrete cracks has been increasingly studied. Typically, self-healing occurs when mineral precipitation takes place in open cracks due to processes such as continued cement hydration and/or carbonation [25,26], secondary reactions of chemical/mineral additives [27–29], and bacterial mineral precipitation [30–32]. Besides the binder composition and water availability, tight crack width strongly promotes self-healing ability. The maximum width for cracks to be able to fully heal varies with concrete types, but is generally below 150 μm [33,34]. This creates a challenge for conventional concrete in which crack widths are normally difficult to reliably control. The ECC materials, however, provide an opportunity for concrete self-healing, particularly due to the autogenously tight crack width, typically below 60 μm irrespective of imposed strains.

The recently developed ECC based on reactive MgO-fly ash blends shows a promise in establishing self-healing ability. The average width of the multiple micro-cracks formed under uniaxial tension measured less than 60 μm [21,22]. The ECC's matrix contains a high volume of reactive MgO, which is not fully reacted during the accelerated CO_2 carbonation. The unreacted MgO and its hydration products create the potential for subsequent dissolution and precipitation in micro-cracks that may facilitate the self-healing process. In an effort to understand the self-healing capability of the MgO-based ECC after carbonation curing, this study employed experimental techniques at multiple scales to assist in characterizing the healing process and products. The outcome of this study complements current understanding regarding durability of the carbonated MgO-ECC material and provides additional insights for lifecycle analysis of energy consumption and carbon emissions.

2. Experiment program

2.1. Materials and specimen preparation

Reactive MgO (MAGOX premium grade, Premier Magnesia, LLC) and Class F fly ash (Headwaters Resources Inc) were used to form a binary system for ECC. Table 1 shows chemical compositions of the raw materials. Polyvinyl alcohol (PVA) fibers (supplied by Kuraray Ltd) with 1.2% oil coating were used and the fiber properties are shown in Table 2. To ensure adequate workability of the fresh ECC mixture, sodium hexametaphosphate (SHMP, chemical formula: $Na(PO_3)_6$) and superplasticizer (SP, ADVA190, W.R. Grace & Co.) were used. All mixtures were prepared with deionized water.

Two mix proportions were considered (M70 and M50, see Table 3), representing high and low MgO dosages (70% and 50% by binder mass), respectively. The fiber dosage was kept at 2% by volume. An SHMP-SP solution was prepared by pre-mixing the two chemicals with mixing water in two steps: (1) add SHMP to the mixing water and stir at 38 rpm at 85 °C for 5 min using a magnetic stirrer, and (2) add SP to the SHMP solution and stir in the same condition for an additional 1 min. The mixing of ECC was conducted in a 4-L mortar mixer. All solid ingredients, *i.e.*, reactive MgO and fly ash, were mixed under dry condition for 2 min at a rate of 16 rpm. The SHMP-SP solution was added to the dry mixture and was mixed at 24 rpm for an additional 3 min. The PVA fibers were then added and mixed for another 5 min to obtain a uniform ECC mixture. The fresh ECC was cast into dogbone-shaped molds (see Fig. 1) and vibrated for 3 min for compaction. Four specimens were prepared for each composite formulation and the average is reported.

After casting, specimens were kept at room temperature for 20 h before demolding. The specimens were air dried for an additional 4 h to achieve a desirable interior moisture condition for CO_2 diffusion, leading to a 24-hour pre-carbonation hydration age. Carbonation was conducted in a pressure vessel continuously filled with CO_2 gas at a constant pressure of 0.2 MPa [21]. As MgO carbonation is a high water absorbing process [4], the internal relative humidity was kept at a minimum of 90% by setting a tray of deionized water below the specimens. ECC specimens were weighed before and after CO_2 carbonation to estimate mass gain induced by the CO_2 uptake process. Detailed procedures and calculations for CO_2 uptake can be can be found in [21].

Table 1
Chemical compositions of reactive MgO and fly ash.

Chemical composition	MgO (%)	Fly ash (%)
SiO_2	0.31	52.19
Al_2O_3	0.2	22.23
SO_3	–	2.16
MgO	95.76	0.93
P_2O_5	–	0.11
K_2O	–	2.56
TiO_2	0.01	1.01
Fe_2O_3	0.13	13.49
CaO	0.81	3.40
LOI at 950 °C	2.75	1.01

Table 2
Physical properties of PVA fiber.

Length (mm)	Diameter (μm)	Elongation (%)	Density (kg/m^3)	Young's modulus (GPa)	Tensile strength (MPa)
8	39	6	1300	42.8	1600

Table 3
Mix proportions of reactive MgO-based ECC (mass ratio).

Batch ID	MgO	Fly ash	Water	SHMP[a]	SP	PVA Fiber[b]
M70	0.7	0.3	0.60	0.060	0.0073	2.0
M50	0.5	0.5	0.52	0.052	0.0073	2.0

[a] SHMP was 10% by water mass.
[b] PVA fiber content was by volume (%).

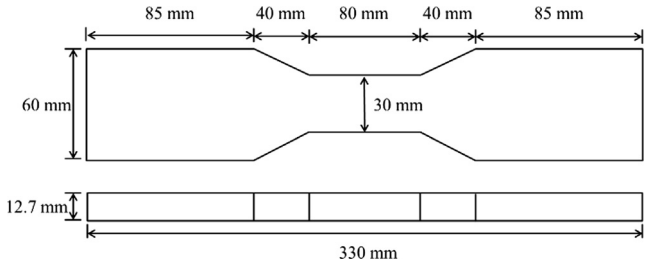

Fig. 1. Dimensions of dogbone-shaped specimen for uniaxial tension test.

2.2. Pre-loading and self-healing

After the curing process, specimens were left to cure in air for 14 days to allow further MgO hydration and strength development. The length of 14 days was experimentally chosen in lieu of the conventional 28 days due to the low hydraulicity of MgO cement, which leads to comparable mechanical binding properties at the two ages. At 14 days, specimens were pre-tensioned to strains of 1%, 1.5% and 2% to generate micro-cracks. An Instron® instrument (ElectroPlus™ E10000 Linear-Torsion Model) with a loading capacity of 10 kN was used at a loading rate of 0.5 mm/min. The tensile deformation was captured by two linear variable displacement transducers mounted at the 80 mm range in the middle of the dogbone-shaped specimens. After achieving the strain level, residual cracks with typical opening widths (30–52 μm [21]) were selectively marked on each specimen to assist in locating the same crack via optical microscopy for crack surface observation during the healing process. The profile of residual cracks in MgO-ECC, including crack numbers and width, can be found in [21].

Self-healing was enabled by a cyclic wetting and drying treatment of the ECC specimens. The pre-loaded specimens were fully immersed in deionized water for 1 day, followed by another day of natural drying in air (RH ~50 ± 5%, temperature ~23 ± 2 °C) to form 1 cycle. Resonance frequency (RF) and specimen mass were used to evaluate the self-healing process. RF was measured at the end of each drying step and specimens were weighed under saturated-surface-dry condition at the end of each wetting step. Optical microscopy observation was conducted using an Infinity X-21 Optical Microscope (resolution: 10 μm, model: Hirbor CX-50470RZ) to capture the crack appearance under the air-dried condition. The total number of wetting and drying cycles was determined by the evolution of specimen mass and RF, with cyclic exposure being terminated when measurements of two adjacent cycles showed a difference less than 10%.

The post-healing tension behavior was assessed to understand the effect of self-healing on ECC mechanical performance. Tension tests followed the same protocol as the pre-loading process described above.

2.3. Characterization of self-healing products

Self-healing is a consequence of a series of physiochemical reactions taking place between matrix materials and ambient environments. Therefore, characterizing the chemical evolution of the matrix material and differentiating it from the healing products is critically important for understanding the mechanisms of the healing process. Samples were extracted from both matrix material and crack-healing products. For the matrix materials, roughly 10 g of solid sample was saw cut and manually ground to pass a 75 μm sieve, whereas the healing products collected from the healed cracks were in the form of fine powders (below 75 μm) and could be directly characterized. The powdered samples were dried in a vacuum desiccator for 7 days using silica gel to remove free water without affecting the bound water that partially forms the binding system.

Thermogravimetric analysis (TGA) coupled with its first derivative (DTG) was used to differentiate healing products from matrix materials. Built upon the different decomposing temperatures where bound water and CO_2 are released, TGA/DTG can provide insights into how the healing products were formed regarding the continuing hydration and carbonation processes. A TA Instruments TGA (SDT650 model) was used for this characterization. Approximately 10 mg of the powdered sample was mounted to a ceramic crucible and was heated from room temperature up to 900 °C at a rate of 10 °C/min. The furnace was purged with pure N_2 gas at a flow rate of 80 ml/min during the heating ramp. Sample mass was continuously recorded and was converted to mass loss curves and DTG curves for phase identification.

The mineralogy of the healing products was characterized using X-ray diffraction (XRD) on the powdered samples collected from the healed cracks. A Rigaku SmartLab XRD with CuKα radiation source was used for the measurement. The X-rays were generated at 40 mA and 45 kV, and the diffraction patterns were captured in 5–70° 2θ with a step size of 0.02° 2θ. MDI Jade 2010 equipped with PDF2004 database was used for mineral phase determination and the results were cross-verified using X'Pert HighScore Plus. The micromorphology of the healing products was observed using a scanning electron microscope (SEM). The images were taken using a Joel IT500 SEM at an accelerating voltage of 10 kV and a magnification at 4000X.

As the optical and SEM observations were limited to the material surface, X-ray computed microtomography (XCT) was used to visualize the interior micro-cracks after the healing process [35]. A ~12.7-mm cube specimen comprising cracks was cut from the pre-loaded dogbone-shaped specimens before the wetting and drying cycles. The cube specimen went through the same cyclic

wet-dry conditions for self-healing and was air dried for 24 h before scanning. The XCT scan was conducted at a tube voltage of 69 kV and a tube current of 147 μA.

3. Results and discussion

3.1. Mass gain, resonance frequency and optical observation

In carbonated MgO-fly ash systems, mass gain is essentially driven by continuous hydration of MgO cement and potential reactions of fly ash, although the reaction degree of fly ash tends to be low due to the weak alkalinity of hydrated MgO. Fig. 2 describes the mass evolution of MgO-ECC during the self-healing process, in which mass gain was observed for both mixes up to 7 wetting and drying cycles. The rate of ECC mass increase was high during the first few cycles and gradually slowed down attaining a total mass change of 1.3% for the M70 mix and 1.0% for the M50 mix at Cycle 7. The higher mass gain in the former is mainly attributed to the high MgO content that takes up more free water through the post-carbonation hydration. Atmospheric carbonation may also contribute to the mass gain, but to a comparatively lesser extent due to the low CO_2 concentration and short period of air exposure. The clear trend of ECC mass increase suggests that the binding phases of the MgO-fly ash blends are still reactive when exposed to the wetting and drying cycles, which is a positive indication of the self-healing capability of this material.

As a typical approach to evaluate the mechanical integrity of solid materials, RF has been widely used for assessing concrete damage, e.g., micro-cracks induced by freeze–thaw cyclic exposure. RF has also demonstrated capability of evaluating self-healing processes of ECC [25,36,37], with a higher RF value often indicating more robust crack filling and higher mechanical integrity after self-healing. Pre-loading poses a significant impact on RF, which is linearly correlated to the pre-loaded strains as shown in Fig. 3. The reductions in RF values with respect to the uncracked specimens (pre-loaded strain at 0%) verified the formation of micro-cracks induced by the pre-tension. Note that the RF measurement was conducted at the unloaded state and therefore reflected the formation of residual cracks rather than the loaded cracks at the imposed strains. Fig. 4 plots the evolution of RF values versus the number of wetting and drying cycles. The RF values were observed to increase rapidly at early cycles of wetting and drying, and progressively approach a plateau after Cycle 6. This suggests that the cracks in ECC were being effectively filled up as the specimens went through the wetting and drying process. As the changes in ECC mass gain and RF value between Cycles 6 and 7 were within 10%, the cyclic exposure was terminated at Cycle

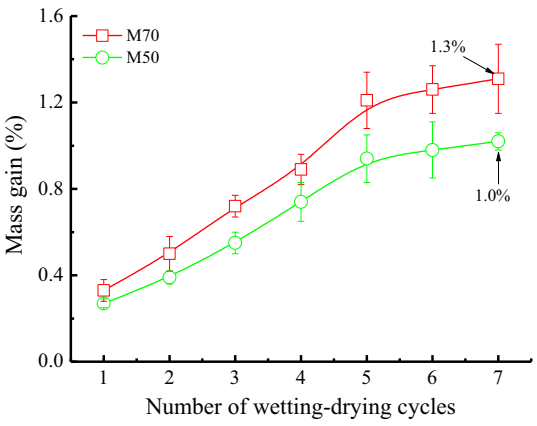

Fig. 2. ECC mass gain during wetting and drying cycles.

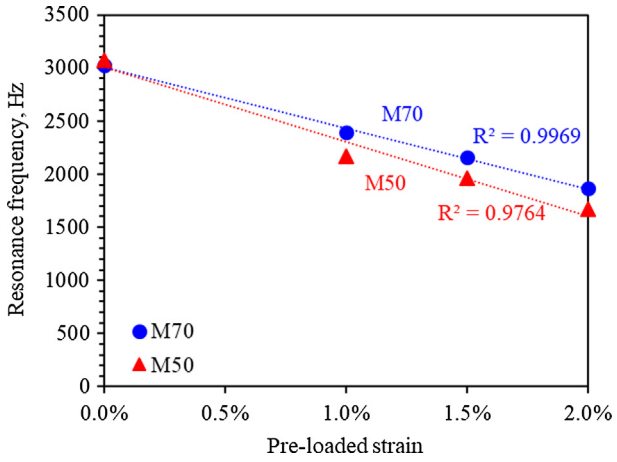

Fig. 3. Linear regression between resonance frequency and pre-loaded strain.

7. The RF ratio was calculated following Eq. (1) [38] and is graphically presented in Fig. 5.

$$\mathrm{RF_{ratio}} = \frac{RF_{precracked}}{RF_{uncracked}} \quad (1)$$

where $\mathrm{RF_{precracked}}$ and $\mathrm{RF_{uncracked}}$ are the RF values measured on the pre-cracked and uncracked ECC specimens after 7 cycles, respectively.

The results of the RF ratios shown in Fig. 5 suggest that both ECC mixes were nearly completely healed after 7 wetting and drying cycles. The M70 specimens, with a higher MgO content, attained comparatively higher RF ratios due to the subsequent MgO hydration that promotes mineral precipitation in crack openings. Nevertheless, both mixes displayed over 95% RF recovery, indicating that the amount of MgO used in the ECC formulations is adequate for enabling the ability to self-heal.

The evolution of ECC RF values could be verified through observations of the crack surface via optical microscopy. Fig. 6 shows the appearance of the crack surface with respect to the number of wetting and drying cycles. The healing products were found to progressively fill in the crack openings with visual confirmation of complete crack sealing by Cycle 7 for both mixes. This observed crack closure after 7 cycles is consistent with the RF results. Mineral precipitation within the cracks would result in a concomitant reduction in crack permeability and potentially retard ingress of detrimental ions and reactive fluids likely to cause further material degradation. In this regard, investigations of post-healing material permeability would be needed to further understand self-healing efficiency in the carbonation-cured system.

3.2. Post-healing tensile properties

The purpose of developing self-healing in construction materials is to (1) seal cracks with solid mineral precipitates in order to retard the pathways for permeation of external detrimental ions and (2) restore material mechanical performance and mitigate composite damages induced by the presence of cracks. In conventional concrete, compressive strength is the main criterion of mechanical performance. In the design framework of ECC (which has radically different applications than conventional concrete), however, tensile strength and ductility represent the key mechanical performance parameters. The composite tensile performance relies on a combination of fiber, matrix and fiber/matrix interfacial properties, and appears less affected by the physical crack packing effect. Therefore, despite the evidence of filled cracks supported by RF ratios and optical microscopy, the post-healing tensile

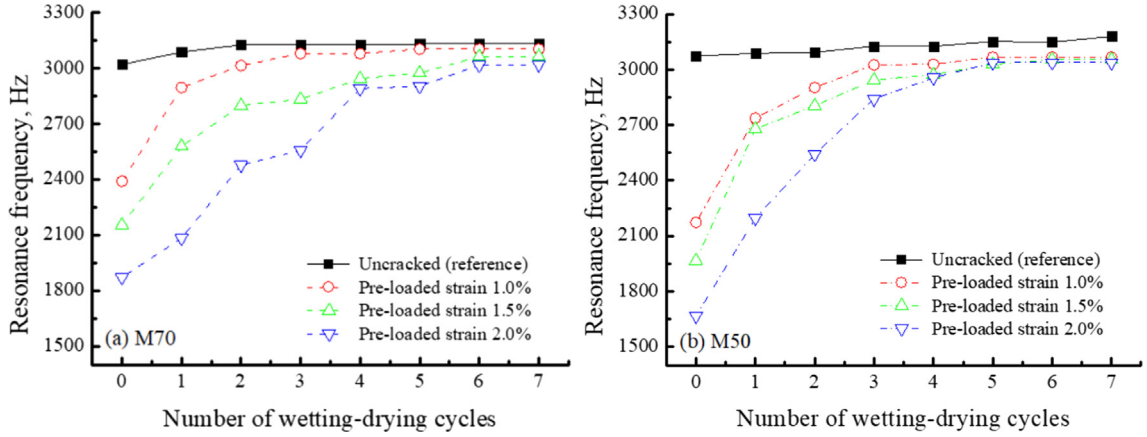

Fig. 4. Evolution of resonance frequency indicating the recovering process of mechanical integrity as a function of wetting and drying cycles, (a) M70, and (b) M50.

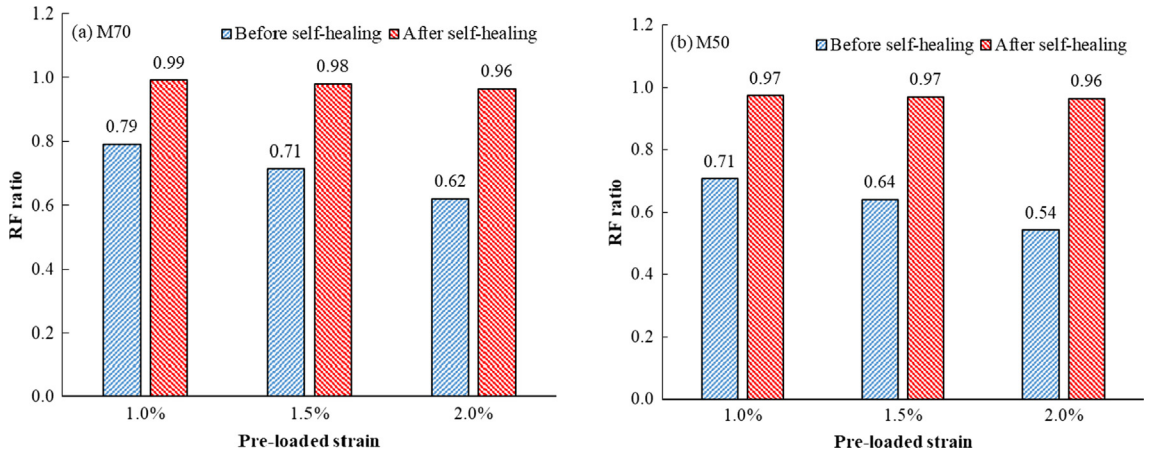

Fig. 5. RF ratios restored to above 95% after self-healing, (a) M70, and (b) M50.

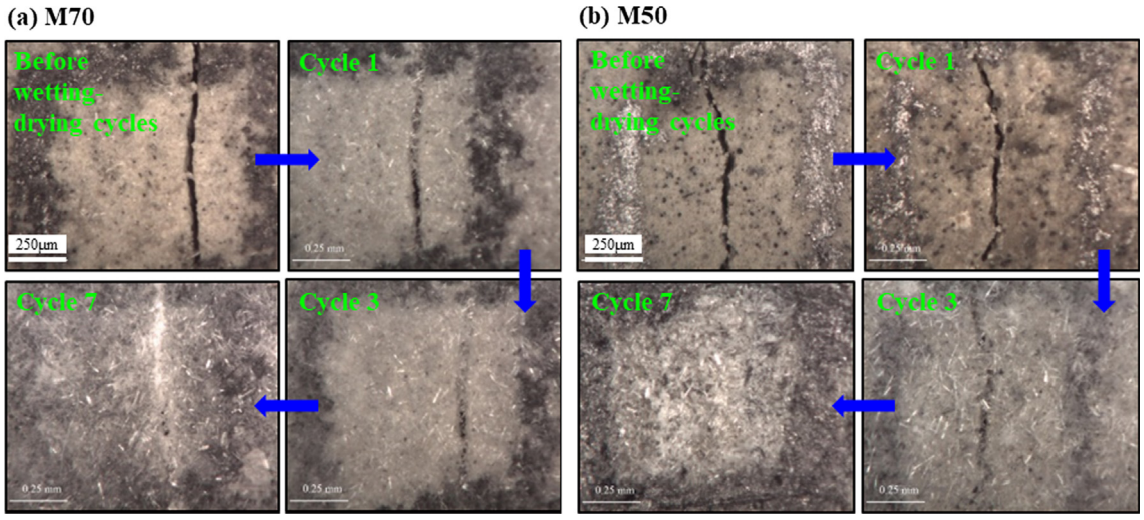

Fig. 6. Crack surface appearance during wetting-drying process under optical microscopy. (a) M70, and (b) M50.

performance of ECC specimens must also be assessed. Uniaxial tension tests were conducted on the specimens after Cycle 7 following the same protocol as that used in pre-loading. Fig. 7 presents the tensile stress-strain relations of the ECC specimens pre-loaded to different strains, together with the uncracked ECC reference after 7 wetting and drying cycles. The tensile strengths and strain capacities are compared in Table 4. It was found that with higher pre-loaded strains specimens tended to exhibit low first-crack strengths and strain capacities. For M70, the first-crack strength decreased from 4.04 MPa for the uncracked reference, to

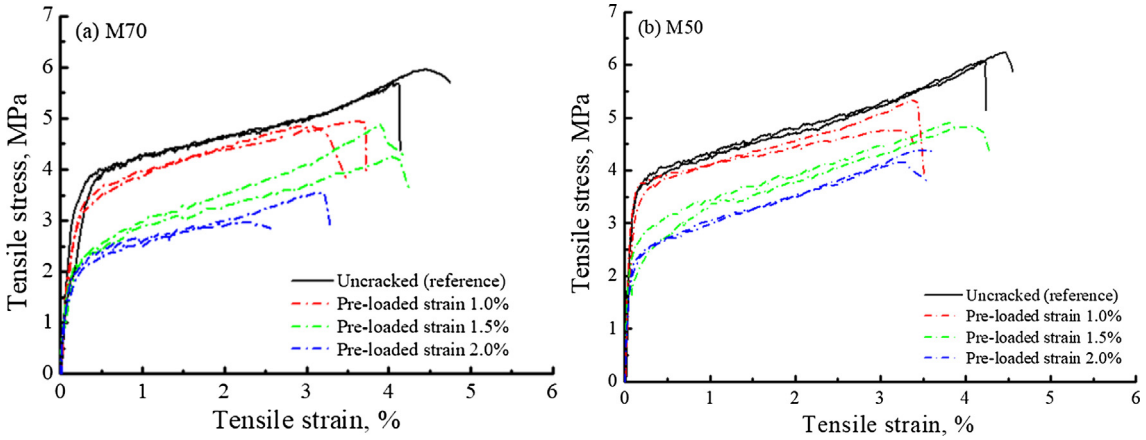

Fig. 7. Uniaxial tensile stress-strain relation of post-healing ECC specimens. (a) M70, and (b) M50. Pre-loaded ECC maintain strain-hardening and ductile behaviors after healing, but with lower tensile strength and strain capacity compared to uncracked reference.

Table 4
Uniaxial tensile properties of post-healing ECC specimens.

Specimen ID and pre-loaded strains		First-crack strength (MPa)	Ultimate tensile strength (MPa)	Tensile strain capacity (%)
M70	Pre-loaded 0%	4.04 ± 0.13	5.76 ± 0.71	4.21 ± 0.55
	Pre-loaded 1.0%	3.80 ± 0.22	4.85 ± 0.18	3.20 ± 0.13
	Pre-loaded 1.5%	3.11 ± 0.14	4.51 ± 0.24	4.05 ± 0.21
	Pre-loaded 2.0%	2.40 ± 0.09	3.34 ± 0.32	2.78 ± 0.17
M50	Pre-loaded 0%	3.93 ± 0.21	6.13 ± 0.62	4.31 ± 0.14
	Pre-loaded 1.0%	3.68 ± 0.15	5.04 ± 0.35	3.34 ± 0.11
	Pre-loaded 1.5%	2.83 ± 0.04	4.85 ± 0.51	3.82 ± 0.18
	Pre-loaded 2.0%	2.14 ± 0.31	4.22 ± 0.63	3.27 ± 0.33

2.40 MPa at a pre-loaded strain of 2%. The post-healing ultimate strength and strain capacity were also reduced by 42% and 34%, respectively. Likewise, M50 ECC followed the same trend after healing, showing up to 31% and 24% lower ultimate tensile strength and strain capacity, respectively, at an imposed pre-loaded strain of 2%. Despite the reductions in tensile strength and ductility, all post-healing ECC specimens displayed typical strain-hardening and ductile characteristics with tensile strain capacity over 2% as depicted in Fig. 7.

Elastic stiffness is a commonly used metric for identifying material resistance to elastic deformation. The post-healing tensile elastic stiffness of ECC specimens is shown in Fig. 8, in which a decreasing trend of the tensile elastic stiffness with the pre-loaded strains was identified. The reduction in tensile elastic stiffness appeared more severe in the M50 ECC, where 2% pre-loaded strain was found to reduce the post-healing stiffness by over 50% compared to the uncracked reference. The post-healing tensile performance suggests that the healing products generated during the wetting and drying cycles were not effective in bridging the cracks under tension, although the crack openings were likely filled up as evidenced by the RF and optical microscopy.

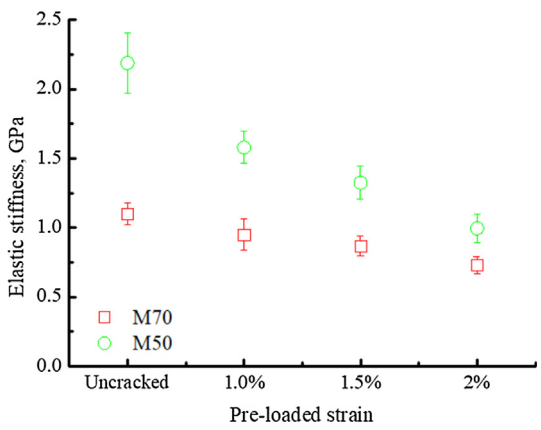

Fig. 8. Tensile elastic stiffness of post-healing ECC specimens.

3.3. Identification of healing products

The mechanical testing and RF measurements suggest that the 'healed' cracks behave differently in forming the tensile integrity compared to the matrix materials in the carbonated MgO-ECC. As such, understanding the constituents of the crack healing products would be useful in identifying new strategies for promoting the robustness of self-healing. TGA coupled with DTG was therefore used to characterize the chemical composition of the healing products and matrix materials. As depicted in Fig. 9**a**, the DTG curves of the matrix materials displayed two major peaks at temperatures of ~90 °C and ~390 °C, corresponding to the dehydration and decarbonation processes, respectively [39]. As the binding properties of the carbonated MgO-fly ash system are attributed to a combination of hydrated magnesium carbonates (HMC) with varying stoichiometry, thermal decomposition of different phases were overlapping and formed two wide peaks on the DTG curves. Generally, the HMCs begin to dehydrate at ~50–100 °C, and fully convert to anhydrous magnesium carbonate at 300 °C [40]. Hydroxyles, however, can sustain higher temperatures and lose bound water up to 350 °C [41]. Fig. 9**b** shows TGA/DTG results of samples extracted from the healed cracks. Healing products from the two mixes displayed nearly identical mass loss and DTG curves, amounting to a total mass loss of ~70% from room temperature to 900 °C. This is substantially higher than the mass loss of matrix materials, suggesting that large amounts of water and CO_2 were

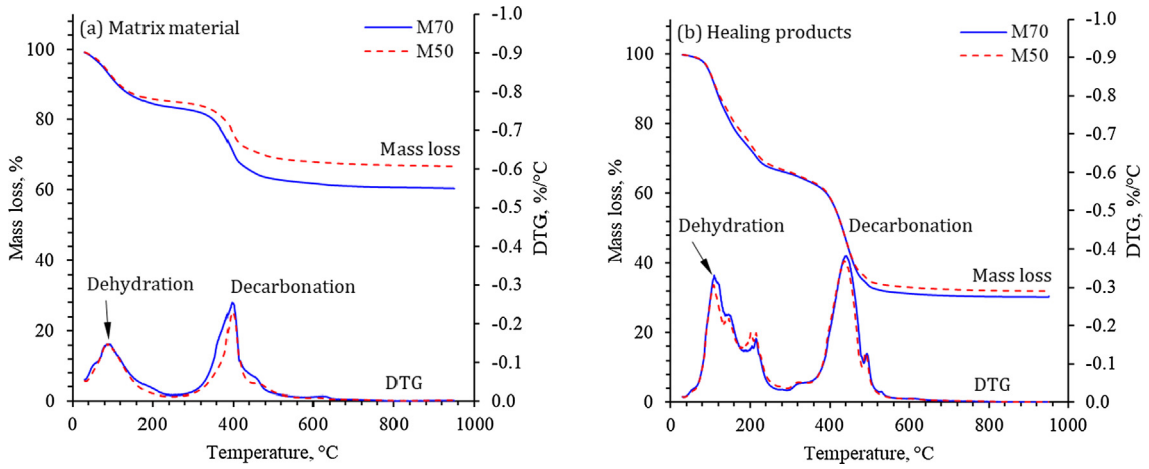

Fig. 9. TGA and DTG for (a) matrix materials, and (b) healing products extracted from filled cracks.

bound during the healing process. Accordingly, the dehydration and decarbonation peaks on the DTG curves showed higher intensities compared to that of matrix materials shown in Fig. 9a. The high mass loss intensities indicate that the healing products potentially contain a high percentage of HMCs.

Due to the peak overlapping of different HMCs on DTG curves, XRD analysis was used to identify minerals present in the crack healing products, as shown in Fig. 10. Peaks of nesquehonite were predominantly identified for both mixes. Hydromagnesite was also detected, but at significantly lower intensities. Note that the formation of nesquehonite (chemical formula: $MgCO_3\,3H_2O$) from MgO binds ~71% H_2O and CO_2 per nesquehonite mass, which correlates well with the TGA mass loss of self-healing products shown in Fig. 9b. This verifies the formation of nesquehonite amongst the HMCs in the crack opening and indicates that nesquehonite is a key contributor to the self-healing identified through optical microscopy and RF observations.

3.4. SEM and XCT images

Experimental results obtained from TGA and XRD suggested that the crystalline nesquehonite filling up the crack openings is responsible for the RF recovery of ECC specimens after the wetting and drying cycles. However, nesquehonite precipitation did not completely restore the cracked ECC, particularly when the healed composite materials were subjected to re-loading, even though complete crack healing was identified under the optical microscopy. Therefore, visualizing the microstructural morphology and crack interior structure would assist in understanding the healing mechanism. Fig. 11 shows the reconstructed XCT image of the ECC specimen after 7 wetting and drying cycles when the cracks were found to have fully healed under optical microscopy. The crack planes, however, were clearly visible in the reconstructed XCT data, indicating a poor healing state throughout the specimen interior. This could be attributed to two factors: (i) the nesquehonite crystallites filling in the cracks were not as dense as the matrix material, hence having a comparatively lower X-ray attenuation that presents as a lighter grayscale coloration in reconstructed images; (ii) self-healing was limited to the material surface, and the interior cracks remained open even after the crack surface healed. Although the two factors were both likely, the former may play the primary role in preventing full healing of the crack. This is evidenced by the recovered RF values in Fig. 4, which would otherwise remain at low levels if there was inconsistent healing between the crack surface and interior. Additionally, differences between the crack surface and interior are not observed in the reconstructed XCT data. The low material density of the healed cracks accounts for the low first-crack strengths in the pre-loaded ECC specimens compared to the uncracked reference. To further exam the micromorphology of healing products, SEM images were taken of the cross section containing healed cracks (see Fig. 12). The microstructure of healing products appeared as elongated needle-like crystallites, consistent with the typical micromorphology of nesquehonite [7]. No flake brucite crystallites or spherical

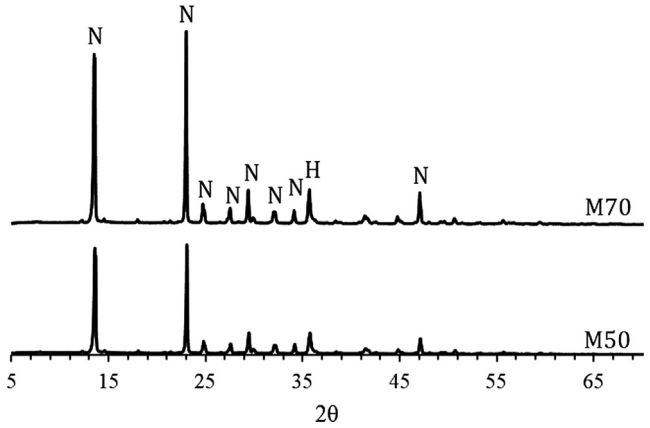

Fig. 10. XRD pattern of healing products extracted from filled cracks. N: nesquehonite, H: hydromagnesite.

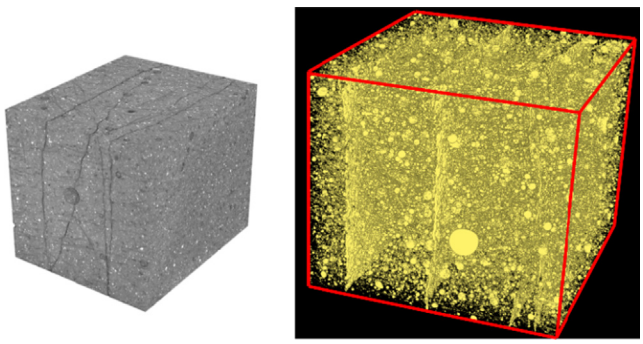

Fig. 11. Reconstructed XCT image segmented to show porosity and micro-cracks in a fully healed ECC specimen under optical microcopy and resonance frequency measurements.

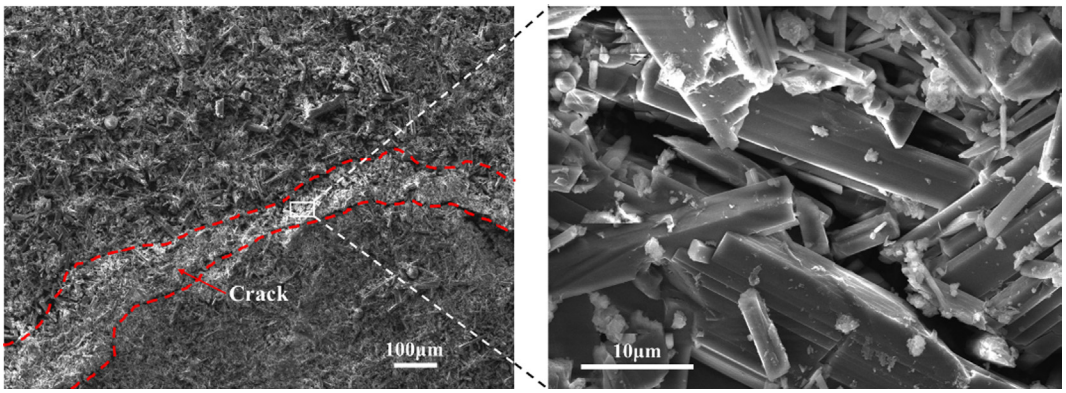

Fig. 12. SEM images showing a healed crack (left) and enlarged morphology of self-healing products inside cracks (right).

fly ash particles were observed in the healing products under SEM, which verifies the XRD data that identified nesquehonite as the primary crack-healing product.

3.5. Healing process

The process of self-healing is graphically illustrated in Fig. 13, where three stages are postulated to account for the self-healing of carbonation-cured MgO-ECC. At the first stage, multiple fine cracks are created by the imposed tensile strain but are kept tight by the fibers bridging across crack openings. After exposure to the wetting and drying cycles, water fills in the cracks and facilitates (1) dissolution of Mg^{2+}, OH^- and CO_3^{2-} ions from the matrix, (2) dissolution of CO_2 from ambient air, and (3) dissolution of a small amount of Ca^{2+} ions from fly ash. As water dries out, the ions crystalize and precipitate solid minerals (mostly HMCs). Given the highest thermodynamic stability of nesquehonite amongst the HMCs in MgO-fly ash-CO_2 systems, mineral precipitation is dominated by nesquehonite needle-shape crystallites of varying dimensions as displayed in Fig. 12. This dissolution and precipitation process (stage II) continues and progressively fills the cracks (see Fig. 6). Fly ash does not seem to affect this healing process, since reaction degrees of fly ash remained at 0 after 7 wetting and drying cycles. Furthermore, the progress of self-healing as reflected by the evolution of RF values and crack surface appearance were found to be similar for ECCs made with 50% and 30% fly ash. The absence of fly ash in the healing products potentially contributes to a lower density of the healing products compared to matrix materials. Although self-healing of the carbonated MgO cements was not capable of adequately bridging the crack openings and recovering mechanical performance under tension, the post-healing ECC specimens still possess strain-hardening characteristics. The healed material may also be less permeable to reactive fluids and have enhanced durability relative to cracked typical MgO-based concrete. Transport properties of healed ECC, particularly when exposed to aggressive environments (e.g., sulfate and acid), need to be further evaluated to address the effectiveness of

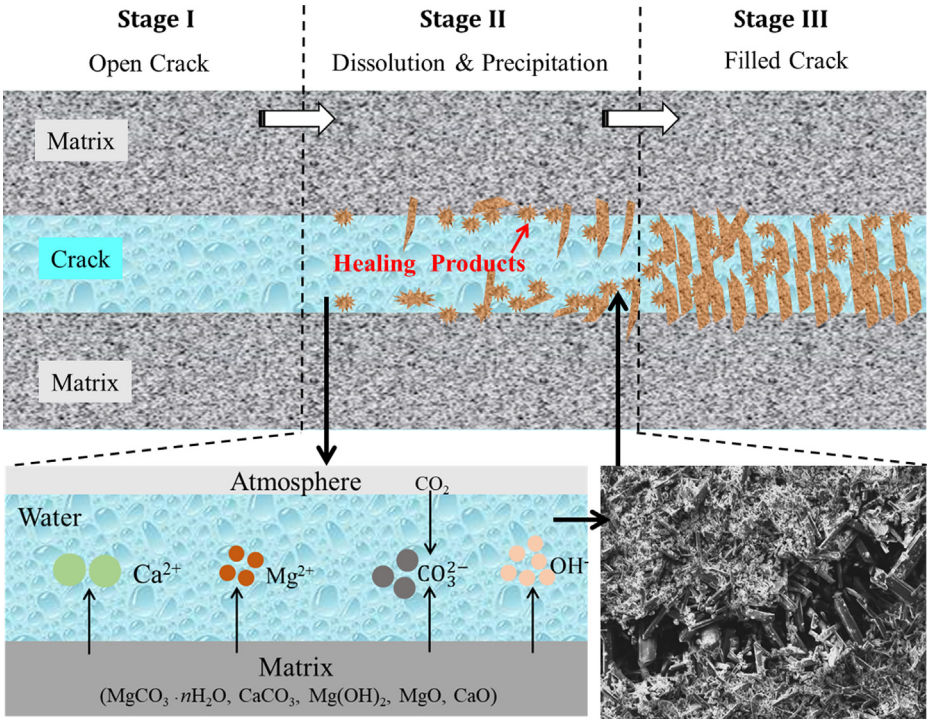

Fig. 13. Illustration of self-healing process of the same crack at different healing stages from left to right. Mineral dissolution and precipitation are responsible for the healing process in carbonation cured MgO-based ECC.

self-healing and to inform material durability design and lifecycle assessment.

4. Conclusions

This study examined the self-healing of Engineered Cementitious Composites (ECC) based on binary blends of reactive MgO cement and fly ash. Wetting and drying cycles were applied as the healing condition. Conclusions are discussed below:

(1) Cracks in the MgO-ECC can be healed in 7 cycles, with over 90% recovery of resonance frequency and fully healed crack surface as observed via optical microscopy. Specimen mass was increased by 1.3% for the ECC with 70% MgO and by 1.0% with 50% MgO, indicating continuing reactions of the MgO cement during the wetting and drying cycles.
(2) The post-healing tensile performance of the MgO-ECC was not fully recovered. Specimens with higher imposed tensile strains tended to show lower tensile strengths, elastic stiffness and strain capacities after the healing process.
(3) The crack opening was clearly identified by XCT imaging after 7 cycles, although optical microscopy suggested complete healing on crack surface. This was in line with the composite tensile performance, collectively indicating that the healing products were different from the matrix material and were not able to mechanically bridge the crack openings in the same manner.
(4) Nesquehonite crystallites were found to be the primary mineral present in the healing products. Fly ash did not play a significant role in the process of self-healing or long-term MgO hydration. To facilitate robust post-healing tensile performance, novel strategies through matrix chemical/mineral modifications or external stimulations are needed.
(5) Resonance frequency may not be accurate in reflecting and predicting composite tensile performance, particularly for MgO-based systems, although it is directly linked to mechanical integrity of materials. In the context of self-healing, characterizations with XCT and post-healing tension experiments are needed for validating the quality of self-healing in MgO-based ECC.

Declaration of Competing Interest

The authors declare that they have no known competing financial interests or personal relationships that could have appeared to influence the work reported in this paper.

Acknowledgements

Financial support for this work was provided by the U.S. Department of Energy, National Energy Technology Laboratory (NETL) through award No. DE-FE0030684.

References

[1] Survey, U.G., Mineral Commodity Summaries, 2019. US Geological Survey, 2019.
[2] T.A. Boden, R.J. Andres, G. Marland, Global, regional, and national fossil-fuel CO2 emissions, carbon dioxide information analysis center, Oak Ridge National Laboratory, U.S. Department of Energy, Oak Ridge, Tenn., USA. Available at https://cdiac.ess-dive.lbl.gov/trends/emis/meth_reg.html. 2017
[3] J. Morrison, G. Jauffret, J.L. Galvez-Martos, F.P. Glasser, Magnesium-based cements for CO2 capture and utilisation, Cement Concr. Res. 85 (2016) 183–191.
[4] D. Zhang, Z. Ghouleh, Y. Shao, Review on carbonation curing of cement-based materials, J. CO2 Util. 21 (2017) 119–131.
[5] A. Al-Tabbaa, Reactive magnesia cement, in: Eco-efficient Concrete, Elsevier, 2013, pp. 523–543.
[6] S.A. Walling, J.L. Provis, Magnesia-based cements: a journey of 150 years, and cements for the future?, Chem Rev. 116 (7) (2016) 4170–4204.
[7] L. Vandeperre, A. Al-Tabbaa, Accelerated carbonation of reactive MgO cements, Adv. Cem. Res. 19 (2) (2007) 67–79.
[8] S. Ruan, C. Unluer, Influence of supplementary cementitious materials on the performance and environmental impacts of reactive magnesia cement concrete, J. Cleaner Prod. 159 (2017) 62–73.
[9] S. Ruan, J. Liu, E.-H. Yang, C. Unluer, Performance and microstructure of calcined dolomite and reactive magnesia-based concrete samples, J. Mater. Civ. Eng. 29 (12) (2017) 04017236.
[10] G. Gadikota, A.-h.A. Park, Accelerated carbonation of Ca-and Mg-bearing minerals and industrial wastes using CO2, in: Carbon Dioxide Utilisation, Elsevier, 2015, pp. 115–137.
[11] C. Unluer, A. Al-Tabbaa, The role of brucite, ground granulated blastfurnace slag, and magnesium silicates in the carbonation and performance of MgO cements, Constr. Build. Mater. 94 (2015) 629–643.
[12] C. Unluer, A. Al-Tabbaa, Enhancing the carbonation of MgO cement porous blocks through improved curing conditions, Cem. Concr. Res. 59 (2014) 55–65.
[13] L. Pu, C. Unluer, Investigation of carbonation depth and its influence on the performance and microstructure of MgO cement and PC mixes, Constr. Build. Mater. 120 (2016) 349–363.
[14] L. Mo, D.K. Panesar, Effects of accelerated carbonation on the microstructure of Portland cement pastes containing reactive MgO, Cem. Concr. Res. 42 (6) (2012) 769–777.
[15] L. Mo, F. Zhang, D.K. Panesar, M. Deng, Development of low-carbon cementitious materials via carbonating Portland cement–fly ash–magnesia blends under various curing scenarios: a comparative study, J. Cleaner Prod. 163 (2017) 252–261.
[16] L. Vandeperre, M. Liska, A. Al-Tabbaa, Microstructures of reactive magnesia cement blends, Cement Concr. Compos. 30 (8) (2008) 706–714.
[17] L. Mo, F. Zhang, M. Deng, D.K. Panesar, Effectiveness of using CO2 pressure to enhance the carbonation of Portland cement-fly ash-MgO mortars, Cement Concr. Compos. 70 (2016) 78–85.
[18] L. Mo, M. Liu, A. Al-Tabbaa, M. Deng, W.Y. Lau, Deformation and mechanical properties of quaternary blended cements containing ground granulated blast furnace slag, fly ash and magnesia, Cem. Concr. Res. 71 (2015) 7–13.
[19] V.C. Li, On, engineered cementitious composites (ECC). A review of the material and its applications, J. Adv. Concr. Technol. 1 (2003) 215–230.
[20] G.A. Keoleian, A. Kendall, J.E. Dettling, V.M. Smith, R.F. Chandler, M.D. Lepech, V.C. Li, Life cycle modeling of concrete bridge design: Comparison of engineered cementitious composite link slabs and conventional steel expansion joints, J. Infrastruct. Syst. 11 (1) (2005) 51–60.
[21] H.-L. Wu, D. Zhang, B.R. Ellis, V.C. Li, Development of reactive MgO-based engineered cementitious composite (ECC) through accelerated carbonation curing, Constr. Build. Mater. 191 (2018) 23–31.
[22] S. Ruan, J. Qiu, E.-H. Yang, C. Unluer, Fiber-reinforced reactive magnesia-based tensile strain-hardening composites, Cement Concr. Compos. 89 (2018) 52–61.
[23] P.K. Mehta, R.W. Burrows, Building durable structures in the 21st century, Indian Concr. J. 75 (7) (2001) 437–443.
[24] M.D. Lepech, V.C. Li, Water permeability of engineered cementitious composites, Cement Concr. Compos. 31 (10) (2009) 744–753.
[25] E.N. Herbert, V.C. Li, Self-healing of microcracks in Engineered Cementitious Composites (ECC) under a natural environment, Materials 6 (7) (2013) 2831–2845.
[26] V.C. Li, E. Herbert, Robust self-healing concrete for sustainable infrastructure, J. Adv. Concr. Technol. 10 (2012) 207–218.
[27] M.A. Sherir, K.M. Hossain, M. Lachemi, The influence of MgO-type expansive agent incorporated in self-healing system of Engineered cementitious Composites, Constr. Build. Mater. 149 (2017) 164–185.
[28] M.A. Sherir, K.M. Hossain, M. Lachemi, Self-healing and expansion characteristics of cementitious composites with high volume fly ash and MgO-type expansive agent, Constr. Build. Mater. 127 (2016) 80–92.
[29] R. Alghamri, A. Kanellopoulos, A. Al-Tabbaa, Impregnation and encapsulation of lightweight aggregates for self-healing concrete, Constr. Build. Mater. 124 (2016) 910–921.
[30] V. Wiktor, H.M. Jonkers, Quantification of crack-healing in novel bacteria-based self-healing concrete, Cement Concr. Compos. 33 (7) (2011) 763–770.
[31] H.M. Jonkers, A. Thijssen, G. Muyzer, O. Copuroglu, E. Schlangen, Application of bacteria as self-healing agent for the development of sustainable concrete, Ecol. Eng. 36 (2) (2010) 230–235.
[32] S. Ruan, J. Qiu, Y. Weng, Y. Yang, J. Chu, C. Unluer, The use of microbial induced carbonate precipitation in healing cracks within reactive magnesia cement-based blends, Cem. Concr. Res. 115 (2019) 176–188.
[33] K. Wang, D.C. Jansen, S.P. Shah, A.F. Karr, Permeability study of cracked concrete, Cem. Concr. Res. 27 (3) (1997) 381–393.
[34] C. Edvardsen, Water permeability and autogenous healing of cracks in concrete, Mater. J. 96 (4) (1999) 448–454.
[35] S. Fan, M. Li, X-ray computed microtomography of three-dimensional microcracks and self-healing in engineered cementitious composites, Smart Mater. Struct. 24 (1) (2014) 015021.
[36] H. Liu, Q. Zhang, C. Gu, H. Su, V. Li, Self-healing of microcracks in Engineered Cementitious Composites under sulfate and chloride environment, Constr. Build. Mater. 153 (2017) 948–956.

[37] Z. Zhang, S. Qian, H. Liu, V.C. Li, Ductile Concrete Material with Self-Healing Capacity for Jointless Concrete Pavement Use, Transport. Res. Rec. J. Transport. Res. Board 2640 (2017) 78–83.
[38] L.L. Kan, H.S. Shi, A.R. Sakulich, V.C. Li, Self-healing characterization of Engineered Cementitious Composite materials, ACI Mater. J. 107 (6) (2010) 617–624.
[39] C. Unluer, A. Al-Tabbaa, Impact of hydrated magnesium carbonate additives on the carbonation of reactive MgO cements, Cem. Concr. Res. 54 (2013) 87–97.
[40] N. Dung, C. Unluer, Sequestration of CO2 in reactive MgO cement-based mixes with enhanced hydration mechanisms, Constr. Build. Mater. 143 (2017) 71–82.
[41] C. Unluer, A. Al-Tabbaa, Characterization of light and heavy hydrated magnesium carbonates using thermal analysis, J. Therm. Anal. Calorim. 115 (1) (2014) 595–607.